

Universal Entanglement Transitions of Free Fermions with Long-range Non-unitary Dynamics

Pengfei Zhang¹, Chunxiao Liu², Shao-Kai Jian³, and Xiao Chen⁴

¹Institute for Quantum Information and Matter and Walter Burke Institute for Theoretical Physics, California Institute of Technology, Pasadena, CA 91125, USA

²Department of Physics, University of California Santa Barbara, Santa Barbara, CA 93106, USA

³Condensed Matter Theory Center and Joint Quantum Institute, Department of Physics, University of Maryland, College Park, MD 20742, USA

⁴Department of Physics, Boston College, Chestnut Hill, MA 02467, USA

Non-unitary evolution can give rise to novel steady states classified by their entanglement properties. In this work, we aim to understand the effect of long-range hopping that decays with $r^{-\alpha}$ in non-Hermitian free-fermion systems. We first study two solvable Brownian models with long-range non-unitary dynamics: a large- N SYK₂ chain and a single-flavor fermion chain, and we show that they share the same phase diagram. When $\alpha > 0.5$, we observe two critical phases with subvolume entanglement scaling: (i) $\alpha > 1.5$, a logarithmic phase with dynamical exponent $z = 1$ and logarithmic subsystem entanglement, and (ii) $0.5 < \alpha < 1.5$, a fractal phase with $z = \frac{2\alpha-1}{2}$ and subsystem entanglement $S_A \propto L_A^{1-z}$, where L_A is the length of the subsystem A . These two phases cannot be distinguished by the purification dynamics, in which the entropy always decays as L/T . We then confirm that the results are also valid for the static SYK₂ chain, indicating the phase diagram is universal for general free-fermion systems. We also discuss phase diagrams in higher dimensions and the implication in measurement-induced phase transitions.

1 Introduction

Unveiling new phases and novel dynamics of quantum many-body systems is one of the most important subjects in condensed matter physics. Recent developments find that a new paradigm exists when we consider non-unitary evolutions. It is found that

Chunxiao Liu: chunxiaoliu@ucsb.edu

Shao-Kai Jian: skjian@brandeis.edu

Xiao Chen: chenaad@bc.edu

for a “hybrid” quantum dynamics composed of both unitary evolution and projective measurement, if we follow the quantum trajectories, the steady state exhibits a transition between a volume-law entangled phase and an area-law entangled phase by varying the measurement strength [1–18]. Later studies show the entanglement transitions also appear in more generalized non-unitary random evolutions [19–24]. In particular, in free-fermion systems, under non-unitary random evolution, there is a stable critical phase, in which the steady state has power-law correlation functions and logarithmic entanglement entropy, with possible entanglement transitions into area-law phases [18, 25–35]. This criticality is attributed to the existence of Goldstone modes from the spontaneous breaking of the continuous symmetry in the enlarged replicated Hilbert space [18, 28, 29].

Most of these studies focus on quantum systems with local interactions. However, most of the state-of-the-art experimental platforms to simulate the quantum many-body dynamics contains intrinsic long-range interactions. For example, the ultracold atoms in the optical lattices interact with a Van der Waals potential $\sim 1/r^6$ and the dipole-dipole interaction in the NMR system decays even slower $\sim 1/r^3$. These long-range interactions can significantly change the ground state property [36, 37] and the quantum dynamics [38–44] under unitary evolution. For example, the Lieb-Robinson bound in local spin chains can receive non-trivial corrections, giving rise to rich lightcone structures depending on the strength of the interaction and the local Hilbert space dimension [38–44]. Consequently, it is not only of great interest but also urgently necessary to correctly incorporate the effect of long-range couplings in non-unitary evolution. Although several papers of numerical simulations of long-range interacting [45, 46] or

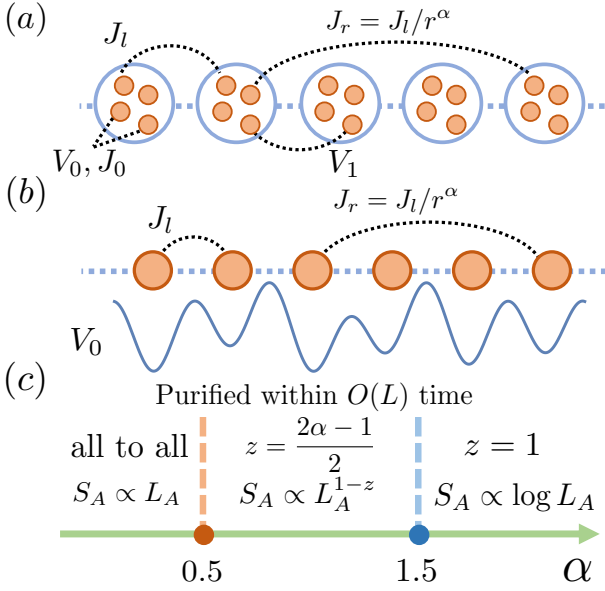


Figure 1: Schematics of (a). The long-range non-hermitian SYK₂ chain. The Hamiltonian is either Brownian or static. (b). Single-flavor chain with imaginary random on-site potential. The randomness is time dependent. In both cases, we use J or V for terms in the H_R or H_I respectively. In particular, J_r represents the long-range hopping. (c). The phase diagram is valid in both models, regardless of the local Hilbert space dimension. Here z is the dynamical exponent and S_A is the entanglement entropy of a subsystem with length L_A .

non-interacting [46] systems under non-unitary evolutions appeared recently, a definite answer of the entanglement properties of non-unitary long-range-coupled random free fermion dynamics is still lacking.

In this work, we present a detailed study on non-unitary free-fermion systems with long-range hopping $J_r \propto 1/r^\alpha$, where r labels the distance between two sites. We investigate this problem by constructing two analytical solvable models in 1-D: the quadratic Brownian Sachdev-Ye-Kitaev (SYK) chain [47–58] with $N \rightarrow \infty$ fermions per site, and a single-flavor $N = 1$ Brownian chain. In both models, the non-unitary evolution can be treated as the free fermion dynamics subject to continuous weak measurements. We will show that such non-unitary dynamics with non-local hopping can stabilize phases with non-trivial correlation and entanglement structure.

The SYK_q model describes N Majorana modes with random q -body couplings [47–49], which is solvable under the large- N expansion. The SYK model has been simulated using nuclear spin chains [59], and a solid-state realization has been proposed

using a graphene flake [60]. Later, different generalizations of the SYK model have been studied, including non-Hermitian Brownian SYK chains in which measurement induced phase transitions can be analyzed using the effective action approach [27–29]. Motivated by these developments, here we use Brownian SYK chains to understand entanglement properties of the steady state under long-range non-unitary evolutions. To test whether the result is sensitive to the large- N limit, we further study the single-flavor Brownian chain using nonlinear master equations [61]. We find that all results match in these models, indicating that the physics is independent of the local Hilbert space dimension. For $\alpha > 0.5$, they show critical behavior and can be further separated into two phases (see FIG. 1). For $\alpha > 1.5$, the long-range hopping decays rapidly enough and the result is the same as the short-range hopping case with dynamical exponent $z = 1$ and logarithmic entanglement entropy. For $0.5 < \alpha < 1.5$, the system is in a fractal phase [21] with subsystem entanglement $S_A \propto L_A^{1-z}$, where L_A is the length of the subsystem A and $z = (2\alpha - 1)/2$. We further confirm that the same result holds for static SYK₂ chain and we propose the phase diagram to be universal for generic non-unitary random free-fermion systems. We also analyze the purification dynamics, where we find the entropy of the system decays as L/T for any arbitrary α .

2 Large- N Model

We first consider the long-range non-Hermitian SYK₂ chain with N Majorana fermions χ^i on each site (see FIG. 1). The Hamiltonian $H = H_R - iH_I$ reads

$$\begin{aligned}
 H_R(t) &= \sum_{x,i,j} i\tilde{J}_{ij}^x(t)\chi_x^i\chi_x^j/2 + \sum_{r \geq 1} \sum_{x,i,j} i\frac{J_{ij}^{x,x+r}(t)}{r^\alpha}\chi_x^i\chi_{x+r}^j, \\
 H_I(t) &= \sum_{x,i,j} \left[iV_{ij}^{x,x+1}(t)\chi_x^i\chi_{x+1}^j + i\tilde{V}_{ij}^x(t)\chi_x^i\chi_x^j/2 \right].
 \end{aligned}
 \tag{1}$$

Here $i, j = 1, 2, \dots, N$ labels the Majorana modes χ on each site and r labels the hopping distance. Here H_I contains intra-site and nearest neighbor hopping, and H_R contains intra-site coupling and long-range hopping. $\tilde{J}_{ij}^x, J_{ij}^{x,x+r}, V_{ij}^{x,x+1}$ and \tilde{V}_{ij}^x are independent random Gaussian variables with zero expectation value. To be concrete, we focus on the Brownian

case with variance

$$\begin{aligned}\overline{\tilde{J}_{ij}^x(t)\tilde{J}_{ij}^x(0)} &= \frac{J_0\delta(t)}{N}, & \overline{V_{ij}^{x,x+1}(t)V_{ij}^{x,x+1}(0)} &= \frac{V_1\delta(t)}{2N}, \\ \overline{\tilde{V}_{ij}^x(t)\tilde{V}_{ij}^x(0)} &= \frac{V_0\delta(t)}{N}, & \overline{J_{ij}^{x,x+r}(t)J_{ij}^{x,x+r}(0)} &= \frac{J_l\delta(t)}{2N}.\end{aligned}\quad (2)$$

For simplicity, we set $J_l = J_0$. Physically, quantum trajectories undergoing non-unitary evolution can be realized by continuous forced measurements as discussed in Appendix E. There are also other related studies of measurements and feedback in quantum many-body systems [62–68]. In particular, in [67], authors find feedback, which gives rise to effective long-memory couplings, can change the critical behaviors.

We are interested in analyzing the steady state under non-unitary evolutions. The system is prepared in some initial state $|\psi_0\rangle$. At time t , the wave function evolves as $|\psi(t)\rangle = e^{-iHt}|\psi_0\rangle / \sqrt{\langle\psi_0|e^{iH^\dagger t}e^{-iHt}|\psi_0\rangle}$. Here we keep any time-ordering operator implicit. Recent studies show phases can be classified according to their entanglement properties [1–25]. We consider the second Rényi entanglement entropy, the definition of which includes two replicas of the original system. We choose a subsystem A with length L_A . The purity of the subsystem A reads

$$P_A = \text{tr}_A(\rho_A)^2 = \frac{\text{tr}_A\left(\text{tr}_B e^{-iHt}|\psi_0\rangle\langle\psi_0|e^{iH^\dagger t}\right)^2}{\left(\langle\psi_0|e^{iH^\dagger t}e^{-iHt}|\psi_0\rangle\right)^2}, \quad (3)$$

where $\text{tr}_{A/B}$ denotes the partial trace of subsystem A or B , and the second Rényi entropy can be obtained as $S_A^{(2)}(t) = -\log P_A(t)$. Previous studies [28, 29] show Keldysh squared correlators, which probe the correlation between two replicas, can also distinguish different phases. It is defined as $F = \sum_{ij} \langle\chi_x^i \chi_0^j\rangle^2 / N$, where

$$\langle\chi_x^i \chi_0^j\rangle \equiv \lim_{t \rightarrow \infty} \frac{\langle\psi_0|e^{iH^\dagger t}e^{-iHt/2}\chi_x^i \chi_0^j e^{-iHt/2}|\psi_0\rangle}{\langle\psi_0|e^{iH^\dagger t}e^{-iHt}|\psi_0\rangle}. \quad (4)$$

Using the fact that the saddle-point solution in the large- N limit is the disorder replica diagonal in the SYK-like models [48, 69, 70], both F [28] and $S_A^{(2)}$ [27, 29, 71–78] can be expressed as a path-integral with two replicas. We begin with the evaluation of $(\langle\psi_0|e^{iH^\dagger t}e^{-iHt}|\psi_0\rangle)^2$. The contour contains four branches (labeled by 1-4), with two forward evolutions (1, 3) and two backward evolutions (2, 4). Here 1 and 2 (3 and 4) belong to the same replica. The

standard derivation [48] leads to the G - Σ action:

$$\begin{aligned}\frac{I}{N} &= -\sum_x \frac{1}{2} \text{tr} \log \left((-1)^{a+1} \delta^{ab} \partial_t - \Sigma_x^{ab} \right) \\ &+ \int_{t_1, t_2} \left[\frac{1}{2} \Sigma_x^{ab} G_x^{ab} + \frac{(-1)^{a+b} \delta(t_{12})}{4} \right. \\ &\times [J_0 (G_x^{ab})^2 + \sum_r \frac{J_0}{r^{2\alpha}} G_x^{ab} G_{x+r}^{ab}] \\ &\left. - \frac{\delta(t_{12})}{4} [V_0 (G_x^{ab})^2 + V_1 G_x^{ab} G_{x+1}^{ab}] \right].\end{aligned}\quad (5)$$

It exhibits $O(2) \times O(2)$ symmetry $G \rightarrow OGO^T$ and $\Sigma \rightarrow O\Sigma O^T$ with $O = \exp(-\gamma_{13}\theta_{13} - \gamma_{24}\theta_{24})$ and $(\gamma_{cd})^{ab} = \delta_{ac}\delta_{bd} - \delta_{bc}\delta_{ad}$. This owes to the enlarge of the permutation symmetry (between 1, 3 or 2, 4) for quadratic actions [28]. In the large- N limit, the saddle point solution for Green's function G_s^{ab} is

$$\begin{aligned}G_s^{11} &= -G_s^{22} = \frac{i\omega}{\omega^2 + \Gamma^2/4}, \\ G_s^{21} &= -G_s^{12} = \frac{\Gamma/2}{\omega^2 + \Gamma^2/4}.\end{aligned}\quad (6)$$

We also have $G_s^{a,b} = G_s^{a-2,b-2}$ for $a, b = 3, 4$, while other components of G_s are zero. Here $\Gamma \equiv V + J$, with $V = V_0 + V_1$ and $J = J_0(1 + \sum_{r=1}^{\infty} 1/r^{2\alpha})$. When $\alpha < 1/2$, the summation diverges and we need to scale J_0 with system size L to obtained a meaningful thermodynamic limit. This indicates the system becomes all-to-all connected, similar to the single SYK₂ model with NL Majorana modes, and the steady state has volume-law entanglement regardless of the strength of the V_0 [71, 74]. For $\alpha > 0.5$, we are able to perform the summation as $J = J_0(1 + \zeta(2\alpha))$, where $\zeta(x)$ is the Riemann zeta function. We will focus on this case in the following discussions.

3 Effective Action

The saddle-point solution G_s breaks the $O(2) \times O(2)$ symmetry down to $O(2)$. Consequently, the fluctuation around the saddle-point contains a gapless Goldstone mode [28, 29]. We consider the fluctuation around saddle-point

$$\begin{aligned}\Sigma(t_1, t_2) &= \Sigma_s(t_1, t_2) + \delta\Sigma(t_1)\delta(t_{12}), \\ G(t_1, t_2) &= G_s(t_1, t_2) + \delta G(t_1, t_2),\end{aligned}\quad (7)$$

and keep to the quadratic order of δG and $\delta\Sigma$. We will focus on components between two replicas as in [28]. Motivated by the symmetry analysis, we define $\theta(t) = \delta G^{14}(t, t)/2$ in the coset space. After

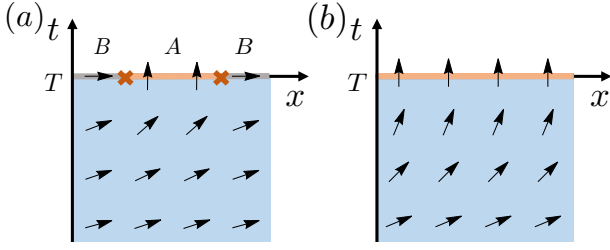


Figure 2: A sketch for the spin configuration (θ is the angle respect to the x -axis) that contributes to the calculation of (a). the second Rényi entanglement entropy on the steady state, (b). the purification dynamics. The cross represents the insertion of the twist operators.

integrating out gapped modes, the effective action derived in Appendix A reads

$$\frac{I_{\text{eff}}}{N} = \frac{1}{2} \int \frac{d\omega dk}{(2\pi)^2} \left(\frac{\epsilon(k)}{2} + \frac{\omega^2}{4V} \right) |\theta(\omega, k)|^2, \quad (8)$$

where the dispersion $\epsilon(k)$ is defined as

$$\epsilon(k) = V_1(1 - \cos(k)) + \sum_{r=1}^{\infty} \frac{J_0}{r^{2\alpha}} (1 - \cos(rk)). \quad (9)$$

Here we have set lattice constant $a_1 = 1$. To determine the low-energy effective theory, we expand $\epsilon(k)$ at small momentum $k \ll 1$. Two possibilities exist depending on α :

$$\epsilon(k) = \begin{cases} C_1 k^2/2 & \text{for } \alpha > 1.5, \\ C_2 k^{2\alpha-1} & \text{for } \alpha \leq 1.5. \end{cases} \quad (10)$$

Here we have $C_1 = V_1 + J_0 \zeta(2\alpha - 2)$ and $C_2 = -J_0 \cos(\frac{1}{2}\pi(1 - 2\alpha)) \Gamma(1 - 2\alpha)$. This can be understood by expanding $(1 - \cos(rk)) \approx k^2 r^2/2$ and realizing the summation is convergent only for $\alpha > 1.5$. The presence of $k^{2\alpha-1}$ for $\alpha < 1.5$ leads to an anomalous action [79], which breaks the conformal symmetry in the replicated Hilbert space. The asymptotic behavior of $\epsilon(k)$ directly determines the dynamical exponent z . We have $z = 1$ for $\alpha > 1.5$ and $z = \frac{2\alpha-1}{2}$ for $\alpha \leq 1.5$.

Now we use the effective action (8) to compute the Keldysh squared correlator F and entanglement entropy $S_A^{(2)}$. On the replicated contour, F corresponds to a four-point correlator of fermions, and thus a two-point function of collective fields θ . More precisely, we have

$$\begin{aligned} F &\sim N \langle \partial_t \theta(x) \partial_t \theta(0) \rangle_{11} \\ &\sim \int_{\omega k} e^{ikx} \frac{\omega^2}{\omega^2 + k^{2z}} \sim x^{-z-1}. \end{aligned} \quad (11)$$

Here we have dropped non-universal factors.

For the entanglement entropy $S_A^{(2)}(T)$, the path-integral contour (3) is defined with additional twist operators at $t = T$, as shown in FIG. 2 (a). In terms of θ , this corresponds to fixing the boundary condition $\theta(T, x \in A) = \pi/2$ and $\theta(T, x \in B) = 0$ [28, 29], which creates a pair of half-vortices, separated by a distance L_A . $S_A^{(2)}$ is equal to the excitation energy of this half-vortex pair. This can be computed by the two-point correlator $P_A \sim \langle e^{i\pi\varphi(L_A)/2} e^{-i\pi\varphi(0)/2} \rangle$. Here $\varphi(x)$ is defined by $\nabla\varphi = N\partial_t\theta/4V$, which shifts the value of $\theta(y)$ for $y < x$. The effective action of φ can be determined by introducing a Lagrangian multiplier r to impose the relation $\nabla\varphi = \partial_t\theta$ and then integrate out θ and r . Working out the details as in Appendix A gives

$$\begin{aligned} S_A^{(2)} &\sim \langle \varphi(L_A) \varphi(0) \rangle \\ &\sim \int_{\omega k} \frac{N}{k^2 + k^{2+2z}/\omega^2} e^{ikL_A} \sim N L_A^{1-z}. \end{aligned} \quad (12)$$

For $z = 1$, this should be understood as $\log L_A$. We find for $0.5 < \alpha < 1.5$, the system is subvolume-law entangled. This is called the fractal phase in [21]. It is straightforward to extend the above discussion to compute the mutual information between two small subregions separated by distance d . The result is $I^{(2)}(d) \sim \langle \nabla\varphi(d) \nabla\varphi(0) \rangle \sim N d^{-z-1}$, which matches the scaling of the squared correlator F .

It is also interesting to ask about the purification dynamics [8] in the free fermion system and check how long it will take to purify the system [80]. We prepare the system in the maximally mixed state and evolve it under the non-unitary dynamics for time T . The second Rényi entropy $S^{(2)}(T)$ of the full system then describes how much the initial quantum information stored in the system is lost [8]. In the effective theory, $S^{(2)}(T)$ is given by computing the energy of the θ field with a boundary condition $\theta(t = 0) = 0$ and $\theta(t = T) = \pi/2$. The dominant contribution is determined by the saddle-point equation $\partial_t^2 \theta = 0$, which gives $\theta(t) = \pi t/2T$. This configuration is shown in FIG. 2 (b), where the spins rotate smoothly from 0 to $\pi/2$. This immediately suggests the purification process is insensitive to the range of the interaction. Explicitly, we have $S^{(2)}(T)/N \sim TL \times 1/T^2 \sim L/T$ and the purification time $\sim O(L)$ for any arbitrary $\alpha \geq 0$.

4 Single-flavor Model

Now we ask whether our results derived in the large- N limit hold for systems with small local Hilbert space dimension. To answer this question, we introduce a second model with single-flavor of fermion per site [81]:

$$H = \sum_{r \geq 1} \left(\frac{J^{x,r+x}(t)}{r^\alpha} c_{x+r}^\dagger c_x + \text{H.C.} \right) - i\kappa_x(t) c_x^\dagger c_x. \quad (13)$$

The first term describes the long-range hopping and the second term is an on-site imaginary potential. Similar to the SYK case, $J^{x,r+x}$ and κ_x are Brownian variables with variance

$$\begin{aligned} \overline{J^{x,x+r}(t) J^{x,x+r}(0)^*} &= J_l \delta(t), \\ \overline{\kappa_x(t) \kappa_x(0)} &= \kappa \delta(t). \end{aligned} \quad (14)$$

We further choose $\kappa = 1$ as the energy unit. At time t ,

$$|\psi(t)\rangle = \frac{e^{-iHt}}{\sqrt{\langle \psi_0 | e^{iH^\dagger t} e^{-iHt} | \psi_0 \rangle}} |\psi_0\rangle. \quad (15)$$

where the initial state $|\psi_0\rangle$ is chosen as a product state in the real space. It is known that under the non-unitary quadratic evolution, $|\psi(t)\rangle$ remains a fermionic Gaussian state [82] and all information is encoded in the correlation function $C_{xy}(t) \equiv \langle \psi(t) | c_x^\dagger c_y | \psi(t) \rangle$. For the Brownian model, it is useful to introduce the distribution function as

$$f_n \equiv \begin{cases} \frac{|C_{x,x}|^2}{L}, & n = 0 \\ \frac{|C_{x,x+n}|^2 + |C_{x,x-n}|^2}{L}, & n > 0 \end{cases}. \quad (16)$$

As in [26], $f_{n>1}$ approximately satisfies a set of non-linear master equation, which takes the form

$$\begin{aligned} \frac{df_n}{dt} &= \mu_n + \sum_{0 < r < n} \frac{J_l}{r^{2\alpha}} (f_{n+r} + f_{n-r} - 2f_n) \\ &+ \sum_{r \geq n} \frac{J_l}{r^{2\alpha}} (f_{n+r} - 2f_n) - 2f_n \sum_{m=1}^{\infty} f_m \\ &+ \sum_{m=1}^{\infty} f_m f_{m+n} + \frac{1}{2} \sum_{m=1}^{n-1} f_m f_{n-m}. \end{aligned} \quad (17)$$

Here the first term $\mu_n = \mu_l/n^{2\alpha}$ is a source term which captures contributions from the diagonal term $C_{x,x}$. The second and the third term are contributions from the Hermitian Brownian hopping and describe a Lévy flight process. Other terms are contributions from the random imaginary fields (see Appendix B)

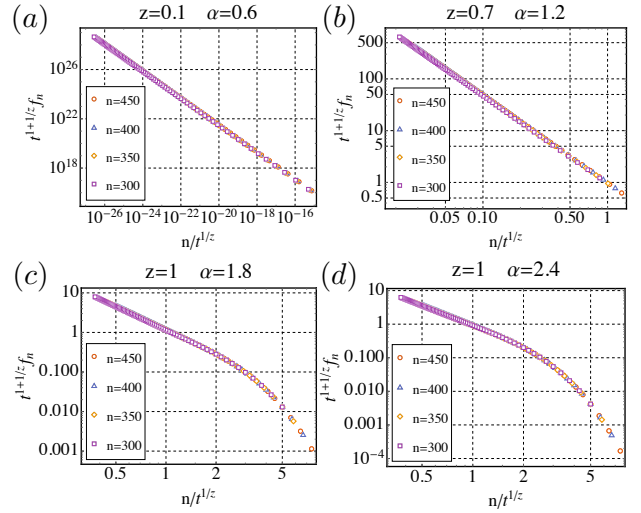


Figure 3: Numerical results obtained by solving the non-linear master equation (17) with $\mu_l = J_l = 1/\zeta(2\alpha)$. We take $t \in [60, 800]$ with a cutoff at $n = 1000$. The slopes for the curves in (a) and (b) are -1.1 and -1.7 respectively. The results show the validity of the scaling form (19).

and is non-linear. For an initial product state, we have $f_{n>1}(0) = 0$.

We aim to understand the dynamics and the long-time behavior of (17). In the short-range hopping limit where $J^{x,x+r} = 0$ for any $r \geq 2$, it is known that the steady state has $f_n \sim 1/n^2$ and the dynamical exponent $z = 1$ [26]. Now we turn on the long-range hopping term. Since the Lévy flight is equivalent to a diffusive random walker when $\alpha > 1.5$, we expect that the entanglement/correlation dynamics is the same as the system with only local hopping term. In this regime, the diffusive term is much slower than the non-linear terms in the master equation and can be safely removed when we analyze the dynamics of the master equation [26].

To determine the physics with $\alpha < 1.5$, we first consider the steady state where $df_n/dt = 0$. The R.H.S. of (17) contains three terms. The contribution from μ_n is proportional to $1/n^{2\alpha}$. Assuming $f_n \sim 1/n^\delta$, the contribution from the imaginary potential gives

$$\int dm f_m (2 \cos(m\partial_n) - 2) f_n \sim 1/n^{2\delta-1}. \quad (18)$$

The steady state is achieved when the contribution from the imaginary potential balances the contribution from μ_n . This gives $\delta = \frac{2\alpha+1}{2}$. For any $\alpha > 0.5$, this guarantees that the Lévy flight terms have larger power-law exponents than the other two terms and can be safely neglected. Assuming the entangle-

ment is contributed by EPR pairs with length distribution described by f_n [30], we can perform a double integral over it to obtain the entanglement entropy $S_A^{(2)} \sim L_A^{(3-2\alpha)/2}$. All these results are consistent with the SYK calculation in the large- N limit.

Now we turn to the determination of the dynamical exponent z in the regime $0.5 < \alpha < 1.5$. At long but finite time t , we expect f_n takes the scaling form:

$$f_n(t) = t^{-\eta} F(n/t^{1/z}). \quad (19)$$

Taking the infinite time limit, we should have

$$f_n(t \rightarrow \infty) \sim t^{-\eta} (nt^{-1/z})^{-\eta z} \sim n^{-\eta z}. \quad (20)$$

Consequently, we have the constraint $\eta z = \delta = \frac{2\alpha+1}{2}$. To determine z , we plug the scaling form (19) into equation (17). It is straightforward to confirm that df_n/dt balances the non-linear convolution term from the imaginary potential¹. We have $df_n/dt \sim 1/t^{\eta+1}$ and

$$\int dm f_m(2 \cos(m\partial_n) - 2)f_n \sim 1/t^{2\eta-1/z}. \quad (21)$$

We conclude $2\eta - 1/z = \eta + 1$ and thus $z = \frac{2\alpha-1}{2}$. This again matches the large- N result. To verify the scaling form (19), we numerically solve the differential equation (17). The results are shown in Fig. 3, from which it is clear that we have $z = 1$ for $\alpha > 1.5$ and $z = \frac{2\alpha-1}{2}$ for $0.5 < \alpha < 1.5$, consistent with our analysis². In particular, we find that the Lévy flight terms can be disregarded (set $J_l = 0$) and does not change the dynamics and the steady state, the same as the master equation with local diffusion term [26].

5 Static Hopping Case

Now we examine whether our phase diagram works for time independent Hamiltonians. The large- N model (1) can be made static by assuming that the random variables are time-independent:

$$\begin{aligned} \overline{(\tilde{J}_{ij}^x)^2} &= \frac{J_0^2}{N}, & \overline{(V_{ij}^{x,x+1})^2} &= \frac{V_1^2}{2N}, \\ \overline{(\tilde{V}_{ij}^x)^2} &= \frac{V_0^2}{N}, & \overline{(J_{ij}^{x,x+r})^2} &= \frac{J_0^2}{2N}. \end{aligned} \quad (22)$$

¹The last two terms in the master equation (17) combine into a convolution term in the continuum limit.

²We also numerically check the purification dynamics and find that $S(T) \sim L/T$, the same as the large- N system.

This model can also be analyzed analogously to the Brownian case (see Appendix C). The main difference is that now the effective action contains copies of Goldstone modes because of the enlarged symmetry due to the time translation symmetry [28]. For each copy, its effective action takes the same form as (8). Consequently, the scaling of the F in (11), the scaling of $S_A^{(2)}$ in (12), and thus phase diagram in FIG. 1 are still valid. We also numerically study the static version of $N = 1$ single-flavor model in (13). Here we take hermitian long-range hopping terms to be time independent while keeping the imaginary potential to be random in the time direction. We manage to numerically reproduce the same result for $\alpha > 1.5$ in Appendix D. Putting all results together, we conclude our phase diagram FIG. 1 is universal for both Brownian and static models, regardless of the local Hilbert space dimension. This is consistent with recent studies [46, 83].

6 Discussions

In this work, we consider the long-range non-unitary random dynamics in free-fermion systems. We analytically show that both the large- N Brownian/static SYK₂ chain and the single-flavor Brownian model exhibit a logarithmic phase for $\alpha > 1.5$ where entanglement is logarithmic in subsystem size, and a fractal phase with $0.5 < \alpha < 1.5$ where the entanglement is subvolume-law. We also show that these two phases cannot be distinguished by the purification dynamics. We expect that the phase diagram is universal for general non-interacting random fermionic systems under long-range non-unitary dynamics. The non-unitary evolution can be interpreted as the dynamics under continuous forced measurements, as explained in Appendix E. An explicit experimental scheme with continuous measurement of particle density on each site has been proposed in [84] using interactions between atoms and photons. Consequently, both entanglement entropy [85] and squared correlator can, in principle, be measured in an experiment with certain post-selection.

We finally make a few comments. Firstly, it is interesting to extend the discussions to general spatial dimension D . For the SYK₂ model, this corresponds to changing the summation over r in (9) to a D -dimensional integral. Consequently, for $\alpha > \frac{2+D}{2}$ we have a phase with $z = 1$, $F(x) = 1/x^{D+1}$ and $S^{(2)} = L_A^{D-1} \log L_A$, while for $\frac{2+D}{2} > \alpha > \frac{D}{2}$, we have $z = \frac{2\alpha-D}{2}$, $F(x) = 1/x^{D+z}$ and $S^{(2)} = L_A^{D-z}$.

Secondly, in [29], authors study the measurement effect on SYK chains by introducing models with two copy of chains with interchain coupling μ . We can construct a similar model with long-range hopping terms. When $\alpha > 0.5$, a transition between the fractal/logarithmic phase and the area law phase occurs at $\mu = J_0(1 + \zeta(2\alpha))$, similar to the observed phase diagram in [46].

Acknowledgment. PZ acknowledges support from the Walter Burke Institute for Theoretical Physics at Caltech. SKJ is supported by the Simons Foundation via the It From Qubit Collaboration. CL is supported by the NSF CMMT program under Grants No. DMR-1818533.

Note added. After this work had been completed, we became aware of an independent investigation of entanglement transition in long-range hopping fermion chains [83].

References

- [1] Xiangyu Cao, Antoine Tilloy, and Andrea De Luca. Entanglement in a fermion chain under continuous monitoring. *SciPost Phys.*, 7:24, 2019. DOI: [10.21468/SciPostPhys.7.2.024](https://doi.org/10.21468/SciPostPhys.7.2.024).
- [2] Yaodong Li, Xiao Chen, and Matthew P. A. Fisher. Quantum zeno effect and the many-body entanglement transition. *Phys. Rev. B*, 98:205136, Nov 2018. DOI: [10.1103/PhysRevB.98.205136](https://doi.org/10.1103/PhysRevB.98.205136).
- [3] Yaodong Li, Xiao Chen, and Matthew P. A. Fisher. Measurement-driven entanglement transition in hybrid quantum circuits. *Phys. Rev. B*, 100:134306, Oct 2019. DOI: [10.1103/PhysRevB.100.134306](https://doi.org/10.1103/PhysRevB.100.134306).
- [4] Brian Skinner, Jonathan Ruhman, and Adam Nahum. Measurement-induced phase transitions in the dynamics of entanglement. *Phys. Rev. X*, 9:031009, Jul 2019. DOI: [10.1103/PhysRevX.9.031009](https://doi.org/10.1103/PhysRevX.9.031009).
- [5] Amos Chan, Rahul M. Nandkishore, Michael Pretko, and Graeme Smith. Unitary-projective entanglement dynamics. *Phys. Rev. B*, 99:224307, Jun 2019. DOI: [10.1103/PhysRevB.99.224307](https://doi.org/10.1103/PhysRevB.99.224307).
- [6] Yimu Bao, Soonwon Choi, and Ehud Altman. Theory of the phase transition in random unitary circuits with measurements. *Physical Review B*, 101(10), Mar 2020. ISSN 2469-9969. DOI: [10.1103/physrevb.101.104301](https://doi.org/10.1103/physrevb.101.104301).
- [7] Soonwon Choi, Yimu Bao, Xiao-Liang Qi, and Ehud Altman. Quantum error correction in scrambling dynamics and measurement-induced phase transition. *Physical Review Letters*, 125(3), Jul 2020. ISSN 1079-7114. DOI: [10.1103/physrevlett.125.030505](https://doi.org/10.1103/physrevlett.125.030505).
- [8] Michael J. Gullans and David A. Huse. Dynamical purification phase transition induced by quantum measurements. *Phys. Rev. X*, 10:041020, Oct 2020. DOI: [10.1103/PhysRevX.10.041020](https://doi.org/10.1103/PhysRevX.10.041020).
- [9] Michael J. Gullans and David A. Huse. Scalable probes of measurement-induced criticality. *Phys. Rev. Lett.*, 125:070606, Aug 2020. DOI: [10.1103/PhysRevLett.125.070606](https://doi.org/10.1103/PhysRevLett.125.070606).
- [10] Chao-Ming Jian, Yi-Zhuang You, Romain Vasseur, and Andreas W. W. Ludwig. Measurement-induced criticality in random quantum circuits. *Phys. Rev. B*, 101:104302, Mar 2020. DOI: [10.1103/PhysRevB.101.104302](https://doi.org/10.1103/PhysRevB.101.104302).
- [11] Aidan Zabalo, Michael J. Gullans, Justin H. Wilson, Sarang Gopalakrishnan, David A. Huse, and J. H. Pixley. Critical properties of the measurement-induced transition in random quantum circuits. *Phys. Rev. B*, 101:060301, Feb 2020. DOI: [10.1103/PhysRevB.101.060301](https://doi.org/10.1103/PhysRevB.101.060301).
- [12] Qicheng Tang and W. Zhu. Measurement-induced phase transition: A case study in the nonintegrable model by density-matrix renormalization group calculations. *Phys. Rev. Research*, 2:013022, Jan 2020. DOI: [10.1103/PhysRevResearch.2.013022](https://doi.org/10.1103/PhysRevResearch.2.013022).
- [13] M. Szyniszewski, A. Romito, and H. Schomerus. Entanglement transition from variable-strength weak measurements. *Phys. Rev. B*, 100:064204, Aug 2019. DOI: [10.1103/PhysRevB.100.064204](https://doi.org/10.1103/PhysRevB.100.064204).
- [14] Lei Zhang, Justin A. Reyes, Stefanos Kourtis, Claudio Chamon, Eduardo R. Mucciolo, and Andrei E. Ruckenstein. Nonuniversal entanglement level statistics in projection-driven quantum circuits. *Physical Review B*, 101(23), Jun 2020. ISSN 2469-9969. DOI: [10.1103/physrevb.101.235104](https://doi.org/10.1103/physrevb.101.235104).
- [15] Shimpei Goto and Ippei Danshita. Measurement-induced transitions of the entanglement scaling law in ultracold gases with controllable dissipation. *Phys. Rev. A*,

- 102(3):033316, 2020. DOI: [10.1103/PhysRevA.102.033316](https://doi.org/10.1103/PhysRevA.102.033316).
- [16] Shao-Kai Jian, Zhi-Cheng Yang, Zhen Bi, and Xiao Chen. Yang-lee edge singularity triggered entanglement transition. *Phys. Rev. B*, 104:L161107, Oct 2021. DOI: [10.1103/PhysRevB.104.L161107](https://doi.org/10.1103/PhysRevB.104.L161107).
- [17] M. Buchhold, Y. Minoguchi, A. Altland, and S. Diehl. Effective theory for the measurement-induced phase transition of dirac fermions. *Phys. Rev. X*, 11:041004, Oct 2021. DOI: [10.1103/PhysRevX.11.041004](https://doi.org/10.1103/PhysRevX.11.041004).
- [18] Yimu Bao, Soonwon Choi, and Ehud Altman. Symmetry enriched phases of quantum circuits. *Annals of Physics*, 435:168618, 2021. ISSN 0003-4916. DOI: <https://doi.org/10.1016/j.aop.2021.168618>. Special issue on Philip W. Anderson.
- [19] Shengqi Sang and Timothy H. Hsieh. Measurement-protected quantum phases. *Phys. Rev. Research*, 3:023200, Jun 2021. DOI: [10.1103/PhysRevResearch.3.023200](https://doi.org/10.1103/PhysRevResearch.3.023200).
- [20] Ali Lavasani, Yahya Alavirad, and Maissam Barkeshli. Measurement-induced topological entanglement transitions in symmetric random quantum circuits. *Nature Physics*, 17(3):342–347, Jan 2021. ISSN 1745-2481. DOI: [10.1038/s41567-020-01112-z](https://doi.org/10.1038/s41567-020-01112-z).
- [21] Matteo Ippoliti, Tibor Rakovszky, and Vedika Khemani. Fractal, logarithmic, and volume-law entangled nonthermal steady states via space-time duality. *Phys. Rev. X*, 12:011045, Mar 2022. DOI: [10.1103/PhysRevX.12.011045](https://doi.org/10.1103/PhysRevX.12.011045).
- [22] Tsung-Cheng Lu and Tarun Grover. Space-time duality between localization transitions and measurement-induced transitions. *PRX Quantum*, 2:040319, Oct 2021. DOI: [10.1103/PRXQuantum.2.040319](https://doi.org/10.1103/PRXQuantum.2.040319). URL <https://link.aps.org/doi/10.1103/PRXQuantum.2.040319>.
- [23] Chao-Ming Jian, Bela Bauer, Anna Keselman, and Andreas W. W. Ludwig. Criticality and entanglement in non-unitary quantum circuits and tensor networks of non-interacting fermions. 12 2020.
- [24] Matteo Ippoliti, Michael J. Gullans, Sarang Gopalakrishnan, David A. Huse, and Vedika Khemani. Entanglement phase transitions in measurement-only dynamics. *Physical Review X*, 11(1), Feb 2021. ISSN 2160-3308. DOI: [10.1103/physrevx.11.011030](https://doi.org/10.1103/physrevx.11.011030).
- [25] O. Alberton, M. Buchhold, and S. Diehl. Entanglement transition in a monitored free-fermion chain: From extended criticality to area law. *Phys. Rev. Lett.*, 126:170602, Apr 2021. DOI: [10.1103/PhysRevLett.126.170602](https://doi.org/10.1103/PhysRevLett.126.170602).
- [26] Xiao Chen, Yaodong Li, Matthew P. A. Fisher, and Andrew Lucas. Emergent conformal symmetry in nonunitary random dynamics of free fermions. *Physical Review Research*, 2(3), Jul 2020. ISSN 2643-1564. DOI: [10.1103/physrevresearch.2.033017](https://doi.org/10.1103/physrevresearch.2.033017).
- [27] Chunxiao Liu, Pengfei Zhang, and Xiao Chen. Non-unitary dynamics of sachdev-ye-kitaev chain. *SciPost Phys.*, 10:48, 2021. DOI: [10.21468/SciPostPhys.10.2.048](https://doi.org/10.21468/SciPostPhys.10.2.048).
- [28] Pengfei Zhang, Shao-Kai Jian, Chunxiao Liu, and Xiao Chen. Emergent Replica Conformal Symmetry in Non-Hermitian SYK₂ Chains. *Quantum*, 5:579, 2021. DOI: [10.22331/q-2021-11-16-579](https://doi.org/10.22331/q-2021-11-16-579).
- [29] Shao-Kai Jian, Chunxiao Liu, Xiao Chen, Brian Swingle, and Pengfei Zhang. Measurement-Induced Phase Transition in the Monitored Sachdev-Ye-Kitaev Model. *Phys. Rev. Lett.*, 127(14):140601, 2021. DOI: [10.1103/PhysRevLett.127.140601](https://doi.org/10.1103/PhysRevLett.127.140601).
- [30] Adam Nahum and Brian Skinner. Entanglement and dynamics of diffusion-annihilation processes with majorana defects. *Physical Review Research*, 2(2), Jun 2020. ISSN 2643-1564. DOI: [10.1103/physrevresearch.2.023288](https://doi.org/10.1103/physrevresearch.2.023288).
- [31] Qicheng Tang, Xiao Chen, and W. Zhu. Quantum criticality in the nonunitary dynamics of (2+1)-dimensional free fermions. *Physical Review B*, 103(17), May 2021. ISSN 2469-9969. DOI: [10.1103/physrevb.103.174303](https://doi.org/10.1103/physrevb.103.174303).
- [32] Alberto Biella and Marco Schiró. Many-body quantum zeno effect and measurement-induced subradiance transition. *Quantum*, 5:528, 2021. DOI: [10.22331/q-2021-08-19-528](https://doi.org/10.22331/q-2021-08-19-528).
- [33] Xhek Turkeshi, Alberto Biella, Rosario Fazio, Marcello Dalmonte, and Marco Schiró. Measurement-induced entanglement transitions in the quantum ising chain: From infinite to zero clicks. *Phys. Rev. B*, 103:224210, Jun 2021. DOI: [10.1103/PhysRevB.103.224210](https://doi.org/10.1103/PhysRevB.103.224210).
- [34] Xhek Turkeshi, Marcello Dalmonte, Rosario Fazio, and Marco Schiró. Entanglement transitions from stochastic resetting of non-hermitian quasiparticles. *arXiv preprint arXiv:2111.03500*, 2021.

- [35] Xhek Turkeshi and Marco Schiró. Entanglement and correlation spreading in non-hermitian spin chains. *arXiv preprint arXiv:2201.09895*, 2022.
- [36] O. Viyuela, D. Vodola, G. Pupillo, and M. A. Martin-Delgado. Topological massive dirac edge modes and long-range superconducting hamiltonians. *Phys. Rev. B*, 94:125121, Sep 2016. DOI: [10.1103/PhysRevB.94.125121](https://doi.org/10.1103/PhysRevB.94.125121).
- [37] Oscar Viyuela, Liang Fu, and Miguel Angel Martin-Delgado. Chiral Topological Superconductors Enhanced by Long-Range Interactions. *Phys. Rev. Lett.*, 120(1):017001, 2018. DOI: [10.1103/PhysRevLett.120.017001](https://doi.org/10.1103/PhysRevLett.120.017001).
- [38] Matthew B. Hastings and Tohru Koma. Spectral gap and exponential decay of correlations. *Communications in Mathematical Physics*, 265(3):781–804, Apr 2006. ISSN 1432-0916. DOI: [10.1007/s00220-006-0030-4](https://doi.org/10.1007/s00220-006-0030-4).
- [39] Takuro Matsuta, Tohru Koma, and Shu Nakamura. Improving the lieb–robinson bound for long-range interactions. In *Annales Henri Poincaré*, volume 18, pages 519–528. Springer, 2017. DOI: [10.1007/s00023-016-0526-1](https://doi.org/10.1007/s00023-016-0526-1).
- [40] Xiao Chen and Tianci Zhou. Quantum chaos dynamics in long-range power law interaction systems. *Physical Review B*, 100(6), Aug 2019. ISSN 2469-9969. DOI: [10.1103/physrevb.100.064305](https://doi.org/10.1103/physrevb.100.064305).
- [41] Chi-Fang Chen and Andrew Lucas. Finite speed of quantum scrambling with long range interactions. *Phys. Rev. Lett.*, 123:250605, Dec 2019. DOI: [10.1103/PhysRevLett.123.250605](https://doi.org/10.1103/PhysRevLett.123.250605).
- [42] Tianci Zhou, Shenglong Xu, Xiao Chen, Andrew Guo, and Brian Swingle. Operator lévy flight: Light cones in chaotic long-range interacting systems. *Phys. Rev. Lett.*, 124:180601, May 2020. DOI: [10.1103/PhysRevLett.124.180601](https://doi.org/10.1103/PhysRevLett.124.180601).
- [43] Minh C. Tran, Andrew Y. Guo, Christopher L. Baldwin, Adam Ehrenberg, Alexey V. Gorshkov, and Andrew Lucas. Lieb-robinson light cone for power-law interactions. *Phys. Rev. Lett.*, 127:160401, Oct 2021. DOI: [10.1103/PhysRevLett.127.160401](https://doi.org/10.1103/PhysRevLett.127.160401).
- [44] Tomotaka Kuwahara and Keiji Saito. Strictly linear light cones in long-range interacting systems of arbitrary dimensions. *Phys. Rev. X*, 10:031010, Jul 2020. DOI: [10.1103/PhysRevX.10.031010](https://doi.org/10.1103/PhysRevX.10.031010).
- [45] Maxwell Block, Yimu Bao, Soonwon Choi, Ehud Altman, and Norman Y. Yao. Measurement-induced transition in long-range interacting quantum circuits. *Phys. Rev. Lett.*, 128:010604, Jan 2022. DOI: [10.1103/PhysRevLett.128.010604](https://doi.org/10.1103/PhysRevLett.128.010604).
- [46] Takaaki Minato, Koudai Sugimoto, Tomotaka Kuwahara, and Keiji Saito. Fate of measurement-induced phase transition in long-range interactions. *Phys. Rev. Lett.*, 128:010603, Jan 2022. DOI: [10.1103/PhysRevLett.128.010603](https://doi.org/10.1103/PhysRevLett.128.010603).
- [47] Alexei Kitaev. A simple model of quantum holography, talk given at the kitp program: entanglement in strongly-correlated quantum matter. *talk given at the KITP Program: entanglement in strongly-correlated quantum matter*, 2015.
- [48] Juan Maldacena and Douglas Stanford. Remarks on the sachdev-ye-kitaev model. *Phys. Rev. D*, 94:106002, Nov 2016. DOI: [10.1103/PhysRevD.94.106002](https://doi.org/10.1103/PhysRevD.94.106002).
- [49] Subir Sachdev and Jinwu Ye. Gapless spin-fluid ground state in a random quantum heisenberg magnet. *Phys. Rev. Lett.*, 70:3339–3342, May 1993. DOI: [10.1103/PhysRevLett.70.3339](https://doi.org/10.1103/PhysRevLett.70.3339).
- [50] Yingfei Gu, Xiao-Liang Qi, and Douglas Stanford. Local criticality, diffusion and chaos in generalized Sachdev-Ye-Kitaev models. *JHEP*, 05:125, 2017. DOI: [10.1007/JHEP05\(2017\)125](https://doi.org/10.1007/JHEP05(2017)125).
- [51] Richard A. Davison, Wenbo Fu, Antoine Georges, Yingfei Gu, Kristan Jensen, and Subir Sachdev. Thermoelectric transport in disordered metals without quasiparticles: The sachdev-ye-kitaev models and holography. *Phys. Rev. B*, 95:155131, Apr 2017. DOI: [10.1103/PhysRevB.95.155131](https://doi.org/10.1103/PhysRevB.95.155131).
- [52] Xin Chen, Ruihua Fan, Yiming Chen, Hui Zhai, and Pengfei Zhang. Competition between chaotic and nonchaotic phases in a quadratically coupled sachdev-ye-kitaev model. *Phys. Rev. Lett.*, 119:207603, Nov 2017. DOI: [10.1103/PhysRevLett.119.207603](https://doi.org/10.1103/PhysRevLett.119.207603).
- [53] Xue-Yang Song, Chao-Ming Jian, and Leon Balents. Strongly correlated metal built from sachdev-ye-kitaev models. *Phys. Rev. Lett.*, 119:216601, Nov 2017. DOI: [10.1103/PhysRevLett.119.216601](https://doi.org/10.1103/PhysRevLett.119.216601).
- [54] Pengfei Zhang. Dispersive sachdev-ye-kitaev model: Band structure and quantum chaos.

- Phys. Rev. B*, 96:205138, Nov 2017. DOI: [10.1103/PhysRevB.96.205138](https://doi.org/10.1103/PhysRevB.96.205138).
- [55] Chao-Ming Jian, Zhen Bi, and Cenke Xu. Model for continuous thermal metal to insulator transition. *Phys. Rev. B*, 96:115122, Sep 2017. DOI: [10.1103/PhysRevB.96.115122](https://doi.org/10.1103/PhysRevB.96.115122).
- [56] Yiming Chen, Hui Zhai, and Pengfei Zhang. Tunable Quantum Chaos in the Sachdev-Ye-Kitaev Model Coupled to a Thermal Bath. *JHEP*, 07:150, 2017. DOI: [10.1007/JHEP07\(2017\)150](https://doi.org/10.1007/JHEP07(2017)150).
- [57] Phil Saad, Stephen H Shenker, and Douglas Stanford. A semiclassical ramp in syk and in gravity. *arXiv preprint arXiv:1806.06840*, 2018.
- [58] Christoph Sünderhauf, Lorenzo Piroli, Xiao-Liang Qi, Norbert Schuch, and J. Ignacio Cirac. Quantum chaos in the Brownian SYK model with large finite N : OTOCs and tripartite information. *JHEP*, 11:038, 2019. DOI: [10.1007/JHEP11\(2019\)038](https://doi.org/10.1007/JHEP11(2019)038).
- [59] Zhihuang Luo, Yi-Zhuang You, Jun Li, Chao-Ming Jian, Dawei Lu, Cenke Xu, Bei Zeng, and Raymond Laflamme. Quantum simulation of the non-fermi-liquid state of sachdev-ye-kitaev model. *npj Quantum Information*, 5(1):1–6, 2019. DOI: [10.1038/s41534-019-0166-7](https://doi.org/10.1038/s41534-019-0166-7).
- [60] Anffany Chen, R. Ilan, F. de Juan, D. I. Pikulin, and M. Franz. Quantum holography in a graphene flake with an irregular boundary. *Phys. Rev. Lett.*, 121:036403, Jul 2018. DOI: [10.1103/PhysRevLett.121.036403](https://doi.org/10.1103/PhysRevLett.121.036403).
- [61] Xiao Chen, Yaodong Li, Matthew PA Fisher, and Andrew Lucas. Emergent conformal symmetry in nonunitary random dynamics of free fermions. *Physical Review Research*, 2(3):033017, 2020.
- [62] Yuto Ashida, Shunsuke Furukawa, and Masahito Ueda. Quantum critical behavior influenced by measurement backaction in ultracold gases. *Phys. Rev. A*, 94:053615, Nov 2016. DOI: [10.1103/PhysRevA.94.053615](https://doi.org/10.1103/PhysRevA.94.053615).
- [63] Yuto Ashida, Shunsuke Furukawa, and Masahito Ueda. Parity-time-symmetric quantum critical phenomena. *Nature communications*, 8(1):1–6, 2017. DOI: [10.1038/ncomms15791](https://doi.org/10.1038/ncomms15791).
- [64] Gabriel Mazzucchi, Wojciech Kozłowski, Santiago F. Caballero-Benitez, Thomas J. Elliott, and Igor B. Mekhov. Quantum measurement-induced dynamics of many-body ultracold bosonic and fermionic systems in optical lattices. *Phys. Rev. A*, 93:023632, Feb 2016. DOI: [10.1103/PhysRevA.93.023632](https://doi.org/10.1103/PhysRevA.93.023632).
- [65] Gabriel Mazzucchi, Santiago F. Caballero-Benitez, Denis A. Ivanov, and Igor B. Mekhov. Quantum optical feedback control for creating strong correlations in many-body systems. *Optica*, 3(11):1213–1219, Nov 2016. DOI: [10.1364/OPTICA.3.001213](https://doi.org/10.1364/OPTICA.3.001213).
- [66] Shrabanti Dhar and Subinay Dasgupta. Measurement-induced phase transition in a quantum spin system. *Phys. Rev. A*, 93:050103, May 2016. DOI: [10.1103/PhysRevA.93.050103](https://doi.org/10.1103/PhysRevA.93.050103).
- [67] D. A. Ivanov, T. Yu. Ivanova, S. F. Caballero-Benitez, and I. B. Mekhov. Feedback-induced quantum phase transitions using weak measurements. *Phys. Rev. Lett.*, 124:010603, Jan 2020. DOI: [10.1103/PhysRevLett.124.010603](https://doi.org/10.1103/PhysRevLett.124.010603).
- [68] Giuseppe Buonaiuto, Federico Carollo, Beatriz Olmos, and Igor Lesanovsky. Dynamical phases and quantum correlations in an emitter-waveguide system with feedback. *arXiv preprint arXiv:2102.02719*, 2021.
- [69] Alexei Kitaev and S. Josephine Suh. The soft mode in the Sachdev-Ye-Kitaev model and its gravity dual. *JHEP*, 05:183, 2018. DOI: [10.1007/JHEP05\(2018\)183](https://doi.org/10.1007/JHEP05(2018)183).
- [70] Yingfei Gu, Alexei Kitaev, Subir Sachdev, and Grigory Tarnopolsky. Notes on the complex Sachdev-Ye-Kitaev model. *JHEP*, 02:157, 2020. DOI: [10.1007/JHEP02\(2020\)157](https://doi.org/10.1007/JHEP02(2020)157).
- [71] Chunxiao Liu, Xiao Chen, and Leon Balents. Quantum entanglement of the sachdev-ye-kitaev models. *Phys. Rev. B*, 97:245126, Jun 2018. DOI: [10.1103/PhysRevB.97.245126](https://doi.org/10.1103/PhysRevB.97.245126).
- [72] Yingfei Gu, Andrew Lucas, and Xiao-Liang Qi. Spread of entanglement in a Sachdev-Ye-Kitaev chain. *JHEP*, 09:120, 2017. DOI: [10.1007/JHEP09\(2017\)120](https://doi.org/10.1007/JHEP09(2017)120).
- [73] Yichen Huang and Yingfei Gu. Eigenstate entanglement in the sachdev-ye-kitaev model. *Phys. Rev. D*, 100:041901, Aug 2019. DOI: [10.1103/PhysRevD.100.041901](https://doi.org/10.1103/PhysRevD.100.041901).
- [74] Pengfei Zhang, Chunxiao Liu, and Xiao Chen. Subsystem Rényi Entropy of Thermal Ensembles for SYK-like models. *SciPost Phys.*, 8:94, 2020. DOI: [10.21468/SciPostPhys.8.6.094](https://doi.org/10.21468/SciPostPhys.8.6.094).
- [75] Arijit Halder, Surajit Bera, and Sumilan Banerjee. Rényi entanglement entropy of Fermi and non-Fermi liquids: Sachdev-Ye-Kitaev model

- and dynamical mean field theories. *Phys. Rev. Res.*, 2(3):033505, 2020. DOI: [10.1103/PhysRevResearch.2.033505](https://doi.org/10.1103/PhysRevResearch.2.033505).
- [76] Pengfei Zhang. Entanglement Entropy and its Quench Dynamics for Pure States of the Sachdev-Ye-Kitaev model. *JHEP*, 06:143, 2020. DOI: [10.1007/JHEP06\(2020\)143](https://doi.org/10.1007/JHEP06(2020)143).
- [77] Yiming Chen, Xiao-Liang Qi, and Pengfei Zhang. Replica wormhole and information retrieval in the SYK model coupled to Majorana chains. *JHEP*, 06:121, 2020. DOI: [10.1007/JHEP06\(2020\)121](https://doi.org/10.1007/JHEP06(2020)121).
- [78] Shao-Kai Jian and Brian Swingle. Note on entropy dynamics in the Brownian SYK model. *JHEP*, 03:042, 2021. DOI: [10.1007/JHEP03\(2021\)042](https://doi.org/10.1007/JHEP03(2021)042).
- [79] Luca Lepori, Davide Vodola, Guido Pupillo, Giacomo Gori, and Andrea Trombettoni. Effective theory and breakdown of conformal symmetry in a long-range quantum chain. *Annals of Physics*, 374:35–66, 2016. DOI: <https://doi.org/10.1016/j.aop.2016.07.026>.
- [80] Lukasz Fidkowski, Jeongwan Haah, and Matthew B. Hastings. How dynamical quantum memories forget. *Quantum*, 5:382, Jan 2021. ISSN 2521-327X. DOI: [10.22331/q-2021-01-17-382](https://doi.org/10.22331/q-2021-01-17-382).
- [81] One may worry about using Majorana fermions in the SYK case but complex fermions in the single-flavor case. In fact, the complex SYK model at half-filling take exactly same entanglement properties as the Majorana SYK model up to a factor of 2. Please see references [71, 74] for more details.
- [82] Sergey Bravyi. Lagrangian representation for fermionic linear optics. *Quantum Info. Comput.*, 5(3):216–238, may 2005. ISSN 1533-7146.
- [83] Thomas Müller, Sebastian Diehl, and Michael Buchhold. Measurement-induced dark state phase transitions in long-ranged fermion systems. *arXiv preprint arXiv:2105.08076*, 2021.
- [84] Hilary M Hurst and IB Spielman. Measurement-induced dynamics and stabilization of spinor-condensate domain walls. *Physical Review A*, 99(5):053612, 2019. DOI: [10.1103/PhysRevA.99.053612](https://doi.org/10.1103/PhysRevA.99.053612).
- [85] Rajibul Islam, Ruichao Ma, Philipp M Preiss, M Eric Tai, Alexander Lukin, Matthew Rispoli, and Markus Greiner. Measuring entanglement entropy in a quantum many-body system. *Nature*, 528(7580):77–83, 2015. DOI: [10.1038/nature15750](https://doi.org/10.1038/nature15750).

A Effective action and Entanglement entropy for the Brownian SYK chain

As we discussed in the main text, we consider the replicated system $(\langle \psi_0 | e^{iH^\dagger t} e^{-iHt} | \psi_0 \rangle)^2$. After introducing bilocal fields and integrating out Majorana fermions, the G - Σ action reads

$$-\frac{I}{N} = \sum_x \frac{1}{2} \text{tr} \log \left((-1)^{a+1} \delta^{ab} \partial_t - \Sigma_x^{ab} \right) - \int_{tt'} \left[\frac{1}{2} \Sigma_x^{ab} G_x^{ab} + \frac{(-1)^{a+b} \delta(t-t')}{4} [J_0 (G_x^{ab})^2 + \sum_r \frac{J_0}{r^{2\alpha}} G_x^{ab} G_{x+r}^{ab}] - \frac{\delta(t-t')}{4} [V_0 (G_x^{ab})^2 + V_1 G_x^{ab} G_{x+1}^{ab}] \right]. \quad (23)$$

We first consider the saddle-point equation for G_x and Σ_x , which reads

$$\begin{aligned} & [(-1)^{a+1} \delta^{ac} \partial_t - \Sigma_x^{ac}] \circ G_x^{cb} = I^{ab}. \\ \Sigma_x^{ab}(t, t') &= V_1 \delta(t-t') \frac{G_{x+1}^{ab}(t, t') + G_{x-1}^{ab}(t, t')}{2} - \sum_{r \geq 1} (-1)^{a+b} \frac{J_0}{r^{2\alpha}} \frac{G_{x+r}^{ab}(t, t') + G_{x-r}^{ab}(t, t')}{2} \\ &+ V_0 G_x^{ab}(t, t') - J_0 (-1)^{a+b} G_x^{ab}(t, t'). \end{aligned} \quad (24)$$

The solution of the equation is translational invariant along space or time $\Sigma_x^{ab}(t, t') = G_s^{ab}(t - t')$. In fact, it takes exactly the same form as the model without long-range hopping [28]:

$$G_s^{11}(\omega) = \frac{i\omega}{\omega^2 + \Gamma^2/4}, \quad G_s^{12}(\omega) = -\frac{\Gamma/2}{\omega^2 + \Gamma^2/4}, \quad (25)$$

We also have $G_s^{a,b} = G_s^{a-2,b-2}$ for $a, b = 3, 4$, while other components of G_s are zero. The effective action can be derived by consider fluctuations around the saddle-point,

$$\Sigma(t_1, t_2) = \Sigma_s(t_1, t_2) + \delta\Sigma(t_1)\delta(t_{12}), \quad G(t_1, t_2) = G_s(t_1, t_2) + \delta G(t_1, t_2), \quad (26)$$

and keep everything to the quadratic order. We will focus on components between two replicas. There are contributions from the $\text{tr} \log$ term, the ΣG term, and the G^2 terms. Comparing to the short-range hopping model [28], the only difference is from the contribution from G^2 terms. Fortunately, these contributions are the simplest ones. As in [28], we introduce

$$\begin{aligned} \phi_1(\omega) &= \sqrt{2} \int dt \delta G^{13}(t, t) e^{i\omega t}, \\ \phi_2(\omega) &= -\sqrt{2} \int dt \delta G^{14}(t, t) e^{i\omega t}. \end{aligned} \quad (27)$$

The G^2 term gives a contribution

$$-\frac{\delta I_{\text{eff}}}{N} = \frac{1}{2} \int_t (V_k (\phi_{1,k} \phi_{1,-k} + \phi_{2,k} \phi_{2,-k}) - J_k (\phi_{1,k} \phi_{1,-k} - \phi_{2,k} \phi_{2,-k})). \quad (28)$$

Here $V_k = V_0 + V_1 \cos(k)$, $J_k = J_0(1 + \sum_r \cos(rk)/r^{2\alpha})$. Adding back contributions from other terms, we have

$$-\frac{I_{\text{eff}}}{N} = \frac{1}{2} \sum_k \int_\omega \phi_k(\omega) \begin{pmatrix} \Gamma - J_k + V_k & -i\omega \\ i\omega & -\Gamma + J_k + V_k \end{pmatrix} \phi_{-k}(-\omega). \quad (29)$$

Denoting $\theta = \sqrt{2}\phi_2$ and integrating out ϕ_1 , we arrive the effective action used in the main text:

$$\frac{I_{\text{eff}}}{N} = \frac{1}{2} \int \frac{d\omega dk}{(2\pi)^2} \left(\frac{\epsilon(k)}{2} + \frac{1}{4V} \omega^2 \right) |\theta(\omega, k)|^2. \quad (30)$$

The squared correlator F corresponds to the two point function of ϕ_1 [28]. In the low energy limit, the equation of motion of ϕ_1 gives $2V\phi_1(\omega) \approx -i\omega\phi_2(\omega)$. This justifies the calculation of F in the main text.

For computing the entanglement entropy, as explained in the main text, we introduce Lagrangian multiplier $r(\omega, k)$ to impose the relation between θ and its dual field φ :

$$I_{\text{eff}} = \int_{\omega k} \frac{N}{2} \left(k^{2z} + \omega^2 \right) |\theta(\omega, k)|^2 + r(\omega, k) (k\theta(\omega, k) + N\omega\varphi(\omega, k)). \quad (31)$$

Here we have dropped non-universal parameters. Integrating out r and θ leads to the effective action of φ used in the main text:

$$\frac{I_{\text{eff}}}{N} = \frac{1}{2N} \int_{\omega k} \left(k^2 + k^{2+2z}/\omega^2 \right) |\varphi(\omega, k)|^2. \quad (32)$$

B Non-linear master equation for the single-flavor model

Now we present the derivation of the non-linear master equation for the single-flavor model. The derivation also follows the short-range hopping case studied in [61].

We first write out the equation satisfied by the correlation matrix C_{xy} . Since the model is Brownian, we can obtain the evolution of $|C_{xy}|^2$ by using the Itô calculus. The derivation is tedious but straightforward [61]. Here we only cite the result. The contribution from the Hermitian long-range hopping part reads

$$\begin{aligned} \left(\frac{d|C_{x,y}|^2}{dt} \right)^{(1)} &= \sum_r \frac{J_l}{r^{2\alpha}} \left\{ |C_{y+r,x}|^2 + |C_{y-r,x}|^2 + |C_{y,x+r}|^2 + |C_{y,x-r}|^2 \right. \\ &\quad - 2\delta_{x,y+r} C_{y+r,y+r} C_{y,y} - 2\delta_{x,y-r} C_{y-r,y-r} C_{y,y} \\ &\quad \left. - 4|C_{x,y}|^2 + 2(C_{x+r,x+r} C_{x,x} + C_{x-r,x-r} C_{x,x}) \delta_{x,y} \right\}. \end{aligned} \quad (33)$$

The contribution from the on-site non-Hermiticity reads

$$\begin{aligned} \left(\frac{d|C_{x,y}|^2}{dt} \right)^{(2)} &= 4|C_{x,y}|^2 + 4|C_{x,y}|^2 \delta_{a,b} - 8|C_{x,y}|^2 (C_{y,y} + C_{x,x}) + 4 \sum_m |C_{y,m}|^2 |C_{m,x}|^2 \\ &\quad + 4 \sum_m [C_{y,m} C_{m,x} C_{m,m} C_{x,y} + C_{x,m} C_{m,y} C_{m,m} C_{y,x}] \\ &\quad - 2 \sum_m [C_{y,m} C_{m,x} C_{x,y} + C_{x,m} C_{m,y} C_{y,x}]. \end{aligned} \quad (34)$$

To study the dynamics of f_n , we rewrite Eq.(33) and Eq.(34) in terms of f_n . Note that this is only possible under certain approximations. The Hermitian part Eq.(33) contributes a term $\sum J_l (f_{n-r} + f_{n+r} - 2f_n)/r^{2\alpha}$. In particular, for $n = r$ this leads to a production of long-range correlation directly from the on-site correlation. For Eq.(34), we follow the discussion in [61] and throw away terms $C_{y,m} C_{m,x} C_{x,y}$ and $C_{y,m} C_{m,x} C_{m,m} C_{x,y}$ when $m \neq x$ or y . The contribution from the on-site imaginary potential then mainly contributes a convolution term $-2f_n \sum_{m=1}^{\infty} f_m + \sum_{m=1}^{\infty} f_m f_{m+n} + \frac{1}{2} \sum_{m=1}^{n-1} f_m f_{n-m}$. Summing up these contributions, we arrive at the master equation used in the main text

$$\begin{aligned} \frac{df_n}{dt} &= \mu_n + \sum_{0 < r < n} \frac{J_l}{r^{2\alpha}} (f_{n+r} + f_{n-r} - 2f_n) + \sum_{r \geq n} \frac{J_l}{r^{2\alpha}} (f_{n+r} - 2f_n) \\ &\quad - 2f_n \sum_{m=1}^{\infty} f_m + \sum_{m=1}^{\infty} f_m f_{m+n} + \frac{1}{2} \sum_{m=1}^{n-1} f_m f_{n-m}, \end{aligned} \quad (35)$$

C The static model

We first consider the static SYK chain with long-range non-Hermitian Hamiltonian. The self-consistent equation for the Green's function reads

$$\begin{aligned} \left[(-1)^{a+1} \delta^{ac} \partial_t - \Sigma_x^{ac} \right] \circ G_x^{cb} &= I^{ab}. \\ \Sigma_x^{ab} &= V_1^2 \frac{G_{x+1}^{ab} + G_{x-1}^{ab}}{2} + V_0^2 G_x^{ab} - (-1)^{a+b} J_0^2 G_x^{ab} - \sum_{l \geq 1} (-1)^{a+b} \frac{J_0^2}{l^{2\alpha}} \frac{G_{x+l}^{ab} + G_{x-l}^{ab}}{2}. \end{aligned} \quad (36)$$

For the saddle-point solution with translational symmetry $G_x^{ab} = G_s^{ab}$. Focusing on the low-energy limit $|\omega| < \frac{2J^2}{\sqrt{J^2+V^2}}$, $G_s(\omega)$ reads

$$G_s^{11}(\omega) = \frac{i\omega}{2J^2}, \quad G_s^{12}(\omega) = -\frac{1}{2J^2} \sqrt{\frac{4J^4}{J^2+V^2} - \omega^2}, \quad (37)$$

together with $G_s^{22}(t) = -G_s^{11}(t)$ and $G_s^{21}(t) = -G_s^{12}(t)$. Here we have defined $V^2 \equiv V_0^2 + V_1^2$ and

$$J^2 = J_0^2 + \sum_{l \geq 1} \frac{J_0^2}{l^{2\alpha}} = J_0^2(1 + \zeta(2\alpha)). \quad (38)$$

Now we turn to the effective action. The $G - \Sigma$ action reads

$$-\frac{I}{N} = \sum_x \frac{1}{2} \text{Tr} \log \left((-1)^{a+1} \delta^{ab} \partial_t - \Sigma_x^{ab} \right) + \int \left[-\frac{1}{2} \Sigma_x^{ab} G_x^{ab} + \frac{1}{4} [V_0^2 (G_x^{ab})^2 + V_1^2 G_x^{ab} G_{x+1}^{ab}] - \frac{(-1)^{a+b}}{4} [J_0^2 (G_x^{ab})^2 + \sum_l \frac{J_0^2}{l^{2\alpha}} G_x^{ab} G_{x+l}^{ab}] \right], \quad (39)$$

Expanding $G_x^{ab}(t, t') = G_s^{ab}(t, t') + \delta G_x^{ab}(t, t')$. We again focus on fluctuations involving two replicas $\{\delta G^{13}, \delta G^{14}, \delta G^{23}, \delta G^{24}\}$ and define $\phi_{\pm} = (\phi_{\pm}^1, \phi_{\pm}^2) = \frac{1}{\sqrt{2}}(\delta G^{13} \pm \delta G^{24}, \delta G^{14} \pm \delta G^{23})$ as in [28], where it is found that only ϕ_+ contributes in the low-energy limit. Keeping to the quadratic order as in the Brownian case, we find the effective action

$$-\frac{I_{\text{eff}}}{N} = \frac{1}{2} \int_{\Omega \omega k} \phi_+(\Omega, \omega, k) \begin{pmatrix} 2V^2 & \frac{i(J^2+V^2)^{3/2}}{2J^2} \Omega \\ -\frac{i(J^2+V^2)^{3/2}}{2J^2} \Omega & -\epsilon(k) + \frac{(J^2+V^2)^2 \Omega^2}{8J^4} \end{pmatrix} \phi_+(\Omega, \omega, k). \quad (40)$$

Here Ω is the center-of-mass frequency and ω is the relative frequency of t and t' . We have

$$\epsilon(k) = (1 - \cos(k))V_1^2 + \sum_{l \geq 1} (1 - \cos(lk))J_l^2 \approx k^2 + k^{2\alpha-1}, \quad (41)$$

which takes the same form as the Brownian case. Integrating out ϕ_+^1 and using the coset variables [28] leads to the anisotropic XY model:

$$\frac{I_{\text{eff}}}{N} = \frac{1}{2} \int_{\Omega \omega k} \left(\frac{2\epsilon(k)}{J^2 + V^2} + \frac{J^2 + V^2}{4J^2V^2} \Omega^2 \right) |\theta^\omega(\Omega, k)|^2. \quad (42)$$

This is the same for as the Brownian case, with an additional label ω for different Goldstone modes. Here we should treat Ω as the frequency in the Brownian case. Consequently, the scaling of the squared correlators and entanglement entropy should be the same as the Brownian model.

D Numerical simulation for $N = 1$

For numerical convenience, we construct a *discrete* non-unitary circuit model for single-flavor free fermion with the evolution operator (unnormalized)

$$U = \prod_{t=1}^T U_\beta(t) U_\tau(t). \quad (43)$$

Here $U_\tau = \exp(-iH_R\tau)$ represents the evolution governed by a long-range hopping Hermitian Hamiltonian H_R and $U_\beta = \exp(-H_I\beta)$ represents the imaginary evolution with Hamiltonian H_I . At time t , we have the wave function

$$|\psi(t)\rangle = \frac{U}{\sqrt{Z}} |\psi(0)\rangle, \quad \text{with } Z = \langle \psi(0) | U^\dagger U | \psi(0) \rangle, \quad (44)$$

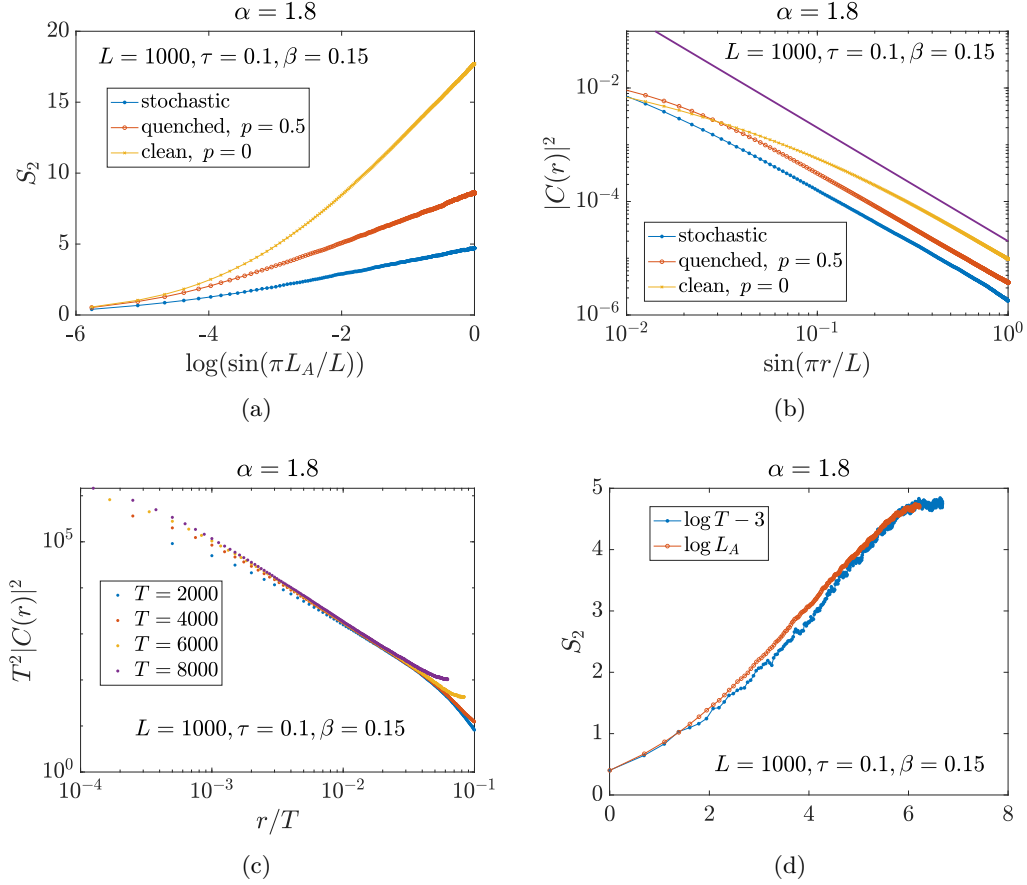


Figure 4: The numerical results at $\alpha = 1.8$ with periodic boundary condition. All the results presented here are averaged over large number of samples. (a) The steady state second Rényi entropy for various non-unitary dynamics. For the blue curve, $J^{x,r+x}$ is a time dependent random variable with the distribution function described by (47). For the red curve, $J^{x,r+x}$ is a time independent random variable with the distribution function described by (48) with $p = 0.5$. For the yellow curve, $J^{x,r+x} = 1$ and H_R has no randomness in it. (b) The steady state squared correlator for various non-unitary dynamics. The color of the curves are the same as that in panel (a). The purple curve is proportional to $1/\sin^2(\pi r/L)$. The blue, red and yellow curves are all parallel to the purple curve, suggesting that the squared correlator decays as $1/r^2$ in all these three models. (c) The data collapse of the squared correlator on the log-log scale. The curves at different times collapse into a single curve, suggesting that $z = 1$. (d) The blue curve is the half system S_2 vs $\log T - 3$ and the red curve is the steady state S_2 vs $\log L_A$. These two curves have the same slope, suggesting that $z = 1$.

where the initial state $|\psi(0)\rangle$ is chosen as a product state in real space. If H_R and H_I are both quadratic Hamiltonians, $|\psi(t)\rangle$ remains a Gaussian state under time evolution. All the information is encoded in the two point correlation function matrix $C_{xy} = \langle \psi(t) | c_x^\dagger c_y | \psi(t) \rangle$.

To incorporate the long-range hopping and periodic boundary condition, we take the following Hamiltonian

$$H_R = \sum_{r \geq 0} \frac{J^{x,r+x}}{1 + \frac{\sin^\alpha(\pi r/L)}{(\pi/L)^\alpha}} (c_{x+r}^\dagger c_x + \text{H.C.}) \quad (45)$$

$$H_I = \kappa_x(t) c_x^\dagger c_x.$$

Here $\kappa_x(t)$ is stochastic random variable with a simple two-component distribution,

$$P(\kappa_x(t)) = \frac{1}{2} \delta(\kappa_x(t) - 1) + \frac{1}{2} \delta(\kappa_x(t) + 1). \quad (46)$$

For the variable $J^{x,r+x}$, we consider two versions: the stochastic and static.

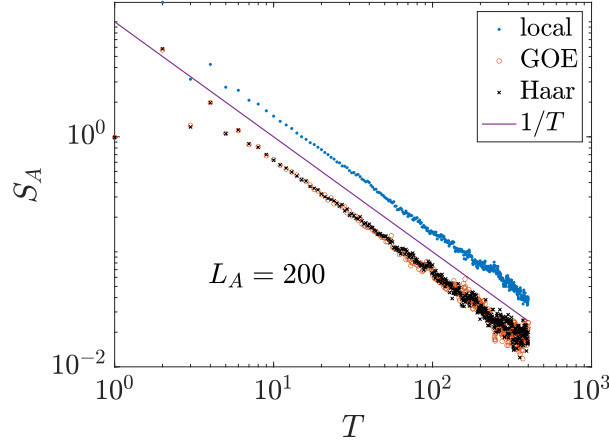


Figure 5: The purification dynamics of non-unitary random dynamics. We take three different unitary evolutions U_τ and we show that the entropies of the system all decay as $1/T$.

In the stochastic case, we take $J^{x,r+x}$ to be a time dependent random variable

$$P(J^{x,r+x}(t)) = \frac{1}{2}\delta(J^{x,r+x}(t) - 1) + \frac{1}{2}\delta(J^{x,r+x}(t) + 1). \quad (47)$$

The numerical results for $\alpha = 1.8$ is shown in Fig. 4. We show that this model has dynamical exponent $z = 1$ and the final steady state has $S_2 \sim \log L_A$ and $C(r) \sim 1/r^2$. We also take H_R to be a time independent Hamiltonian with $J^{x,r+x}$ satisfying

$$P(J^{x,r+x}) = p\delta(J^{x,r+x} - 1) + (1 - p)\delta(J^{x,r+x} + 1). \quad (48)$$

We present the steady state results for $p = 0$ and $p = 0.5$ in Fig. 4 (a) (b). Notice that when $p = 0$, H_R is a clean system without disorder. They all have the same scaling behavior as the stochastic version. We also try other $\alpha > 1.5$ and we obtain the same results. These numerical simulation results suggest that the discrete dynamics has the same result as the Brownian dynamics we discussed in the main text in the regime $\alpha > 1.5$. However, we are unable to obtain consistent numerical results for $\alpha < 1.5$ due to strong finite size effect with $L = 1000$.

D.1 Purification dynamics

We also take the initial system A as a density matrix and study how fast it can purify under non-unitary random dynamics. We take the unitary dynamics U_τ to be random in the spatial and time direction and H_I to be a stochastic random potential term. We consider three different cases for unitary dynamics : a local Hamiltonian for H_R , a single-particle Gaussian orthogonal ensemble (GOE) random matrix for H_R and single-particle Haar random matrix for U_τ . As shown in Fig. 5, in all these cases, the system A has the second Rényi entropy $S_A \sim 1/T$, regardless of the locality structure of U_τ .

E The realization of non-unitary dynamics

In this section, we discuss the experimental relevance of our work by relating the single quantum trajectory under the non-unitary evolution to evolution with continuously forced measurements. We focus on the single-flavor model where

$$H_I = \sum_x \kappa_x(t) c_x^\dagger c_x. \quad (49)$$

After having generated a set of random numbers for $\kappa_x(t)$, we can make a constant shift of the potential such that $\kappa_x(t) > 0$. This is due to the particle number conservation of the system.

Intuitively, such imaginary potential terms should correspond to measuring the on-site particle numbers. We hope to make such relation explicit. To begin with, we consider continuously monitoring our system: at each time step dt , we apply a measurement at site x . The measurement is described by a set of operators

$$\{M_x^0, M_x^1\} = \left\{ 1 - s_x(t)c_x^\dagger c_x, \sqrt{2s_x(t) - s_x(t)^2}c_x^\dagger c_x \right\}. \quad (50)$$

Here we assume $0 < s_x(t) \ll 1$, which means the measurement strength is weak. It is straightforward to check the completeness relation $\sum_i M_x^i (M_x^i)^\dagger = I$. For a system in some density matrix $\rho(t)$ before the measurement, after a single measurement, depending on the outcome, the unnormalized density matrix becomes

$$\rho^0(t+dt) = M_x^0 \rho(t) (M_x^0)^\dagger, \quad \rho^1(t+dt) = M_x^1 \rho(t) (M_x^1)^\dagger. \quad (51)$$

And the probability for obtaining $\rho^i(t+dt)$ is given by $p^i = \text{tr}[\rho^i(t+dt)]$. For forced measurement, we only keep the result when the outcome is 0. Then the evolution of the unnormalized density matrix is given by

$$\rho(t+dt) = M_x^0 \rho(t) M_x^0 \approx \rho(t) - s_x(t)c_x^\dagger c_x \rho(t) - \rho(t)s_x(t)c_x^\dagger c_x + o(s_x) \quad (52)$$

Here we have kept only terms up to $O(s_x)$. Now we choose $s_x(t) = \kappa_x(t)dt$, the evolution can now be written as

$$\rho(t+dt) = e^{-\kappa_x(t)c_x^\dagger c_x dt} \rho(t) e^{-\kappa_x(t)c_x^\dagger c_x dt} + O(dt^2). \quad (53)$$

After adding up measurements over all sites, this matches the result of non-Hermitian Hamiltonian dynamics.

The traditional n -th subsystem Rényi entropy $S_A^{(n)}$ is defined as

$$S_A^{(n)} = -\frac{1}{(n-1)} \text{tr} \rho \log \left(\frac{\text{tr}_A (\text{tr}_B \rho)^n}{(\text{tr} \rho)^n} \right) = -\frac{1}{(n-1)} \log \left(\frac{\text{tr} [\rho \otimes \rho \dots \otimes \rho \mathcal{X}_A]}{\text{tr} [\rho \otimes \rho \dots \otimes \rho]} \right). \quad (54)$$

In particular, the second Rényi entropy $S_A^{(2)}$ has been measured in experiments [85] for systems under unitary evolution. We have written the Rényi entropy as the expectation of the replicated system. Here \mathcal{X}_A is the cyclic permutation operator for subsystem A .

We further show that $S_A^{(n)}$ can in principle be measured directly in experiments by generalization protocols in [85]. For simplicity, we again focus on the $n = 2$ case and analyze the effect of a single measurement. We prepare two copies of systems in some initial state $\rho(t) \otimes \rho(t)$. We now measure the system using operators $M_x^i \otimes M_x^j$:

$$\{M_x^0 \otimes M_x^0, M_x^1 \otimes M_x^0, M_x^0 \otimes M_x^1, M_x^1 \otimes M_x^1\}. \quad (55)$$

The probability of getting ij is given by $\text{tr} [\rho^i \otimes \rho^j]$. We now post select results with $i = j = 0$ only. The probability of getting result ii and the normalized state after getting the result are then given by

$$\rho_d = \frac{\rho \otimes \rho}{\text{tr} [\rho \otimes \rho]}. \quad (56)$$

The swap operator \mathcal{X}_A can be measured by applying additional Rabi oscillations between replicas [85]. This leads to

$$\langle \mathcal{X}_A \rangle = \text{tr} [\mathcal{X}_A \rho_d] = \frac{\text{tr} [\rho \otimes \rho \mathcal{X}_A]}{\text{tr} [\rho \otimes \rho]}, \quad (57)$$

which directly gives $e^{-\tilde{S}_A^{(2)}}$. Note that this experimental realization faces the same challenge in the mixed unitary-measurement dynamics described in Refs. [1–18].